Research Square

Preprints are preliminary reports that have not undergone peer review.
They should not be considered conclusive, used to inform clinical practice,
or referenced by the media as validated information.

Succinate ameliorates motor and gastrointestinal dysfunction in Parkinson's disease by activating PI3K/Akt/mTOR Pathway via gut microbiota modulation

Yue-Qi Jiang
Chinese Academy of Medical Sciences & Peking Union Medical College
Shou-Peng Cao
Chinese Academy of Medical Sciences & Peking Union Medical College
Jun-Mei Shang
Chinese Academy of Medical Sciences & Peking Union Medical CollegeDepartment of Pharmacy, State Key Laboratory of Complex Severe and Rare Diseases, Peking Union Medical College Hospital,
Mei-Chuan Zhou
Chinese Academy of Medical Sciences & Peking Union Medical College
Sen-Xiang Zeng
Chinese Academy of Medical Sciences & Peking Union Medical College
Jin-Rong Wang
Chinese Academy of Medical Sciences & Peking Union Medical College
Yi-Rong Dong
Chinese Academy of Medical Sciences & Peking Union Medical College
Hui-Qing Mi
Chinese Academy of Medical Sciences & Peking Union Medical College
Jia-Hui Wang
Chinese Academy of Medical Sciences & Peking Union Medical College
Rui-Bin Yao
Capital Medical University
Hui-Quan Guo
Chinese Academy of Medical Sciences & Peking Union Medical College
Jia-Lei Wang
Chinese Academy of Medical Sciences & Peking Union Medical College
Ze-Ming Wang
Chinese Academy of Medical Sciences & Peking Union Medical College
Chen Chen
Chinese Academy of Medical Sciences & Peking Union Medical College
Yang Yang

Chinese Academy of Medical Sciences & Peking Union Medical College

Fang-Fang Li

Chinese Academy of Medical Sciences & Peking Union Medical College

Xiu-Qi Bao

Chinese Academy of Medical Sciences & Peking Union Medical College

Cai-Xia Zang

Chinese Academy of Medical Sciences & Peking Union Medical College

Dan Zhang

danzhang@imm.ac.cn

Chinese Academy of Medical Sciences & Peking Union Medical College

---

Article

Keywords: Parkinson’s disease, Energy metabolism, Tricarboxylic acid cycle, Gut microbiota, Succinate

Posted Date: November 25th, 2026

DOI: https://doi.org/10.21203/rs.3.rs-11590669/v1

License: This work is licensed under a Creative Commons Attribution 4.0 International License.
Read Full License

Additional Declarations: No competing interests reported.

Succinate ameliorates motor and gastrointestinal dysfunction in Parkinson's disease by activating PI3K/Akt/mTOR Pathway via gut microbiota modulation

Yue-Qi Jiang[a#], Shou-Peng Cao[a#], Jun-Mei Shang[b#], Mei-Chuan Zhou[a], Sen-Xiang Zeng[a], Jin-Rong Wang[a], Yi-Rong Dong[a], Hui-Qing Mi[a], Jia-Hui Wang[a], Rui-Bin Yao[c], Hui-Quan Guo[a], Jia-Lei Wang[a], Ze-Ming Wang[a], Chen Chen[a], Yang Yang[a], Fang-Fang Li[a], Xiu-Qi Bao[a], Cai-Xia Zang[a]*, Dan Zhang [a]*

[a] State Key Laboratory of Bioactive Substance and Function of Natural Medicines, Department of Pharmacology, Institute of Materia Medica, Chinese Academy of Medical Sciences & Peking Union Medical College, 1 Xian Nong Tan Street, Beijing 100050, P. R. China.

[b] Department of Pharmacy, State Key Laboratory of Complex Severe and Rare Diseases, Peking Union Medical College Hospital, Chinese Academy of Medical Sciences and Peking Union Medical College, Beijing, China, 100730.

[c] Capital Medical University, Beijing, China.

[#]Co-first authors

*Corresponding authors: Cai-Xia Zang (E-mail: zangcaixia@imm.ac.cn), Dan Zhang (E-mail: danzhang@imm.ac.cn).

E-mail address:

Yue-Qi Jiang: yueqi_jiang@163.com

Shou-Peng Cao: caoshoupeng@imm.ac.cn

Jun-Mei Shang: m18634928390@163.com

Mei-Chuan Zhou: zhoumeichuan@imm.ac.cn

Sen-Xiang Zeng: zengsenxiang@imm.ac.cn

Jin-Rong Wang: wangjinrong@imm.ac.cn

Yi-Rong Dong: dongyirong@imm.ac.cn

Hui-Qing Mi: mihuiqing@imm.ac.cn

Jia-Hui Wang: wjiahui@imm.ac.cn

Rui-Bin Yao: 13511076942@163.com

Hui-Quan Guo: guohuiquan@imm.ac.cn

Jia-Lei Wang: wangjialei@imm.ac.cn

Ze-Ming Wang: wangzeming@imm.ac.cn

Chen Chen: chenchen2026@imm.ac.cn

Yang Yang: yangy@imm.ac.cn

Fang-Fang Li: lifangfang@imm.ac.cn

Xiu-Qi Bao: baoxiuqi@imm.ac.cn

Cai-Xia Zang: zangcaixia@imm.ac.cn

Dan Zhang: danzhang@imm.ac.cn

Abstract: Parkinson's disease (PD) is closely associated with mitochondrial dysfunction and impaired energy metabolism, with gut microbiota dysbiosis acting as a critical initiating event that drives disease progression via the disrupted microbiota–gut–brain axis. However, how gut microbiota disturbance affects bioenergy homeostasis in the brain and drives PD pathogenesis remains largely unclear. In the present study, we found that microbiota dysbiosis and gastrointestinal dysfunction occurred prior to motor impairment and dopaminergic neurodegeneration in α-synuclein (A53T) mice. Multi-omics analysis identified tricarboxylic acid (TCA) cycle imbalance as a core metabolic feature of PD, and succinate was characterized as a key microbial metabolite linking gut dysbiosis and central energy metabolic abnormalities. Further functional verification demonstrated that succinate treatment ameliorated motor deficits, gastrointestinal dysfunction, and TCA disturbance in rotenone-induced PD mice. Mechanistically, succinate alleviated PD pathologies and energy imbalance by activating the PI3K/Akt/mTOR signaling pathway. Collectively, our findings demonstrated that gut microbiota dysbiosis and TCA cycle imbalance represent key pathological divers of PD progression. As a vital intermediate of TCA cycle and a gut microbiota-derived metabolite, succinate bridged gut microbial and energy metabolism to mitigate PD pathological damage. These findings provided novel insights into PD pathogenesis and potential therapeutic targets.

Keywords: Parkinson's disease, Energy metabolism, Tricarboxylic acid cycle, Gut microbiota, Succinate

Abbreviation: PD, Parkinson's disease; α-syn, α-synuclein; ATP, adenosine triphosphate; TCA, tricarboxylic acid cycle; GI, gastrointestinal; PI3K, phosphoinositide 3-kinase; Akt, protein kinase B; mTOR, mammalian target of rapamycin; WT, wild type; CMC-Na, carboxymethylcellulose sodium; OTU, operational taxonomic unit; ASV, amplicon sequence variant; PICRUSt2, phylogenetic investigation of communities by reconstruction of unobserved states 2; KEGG, kyoto encyclopedia of genes and genomes; GO, gene ontology; NO, nitric oxide; ANOVA, analysis of variance; ANOSIM, analysis of similarities; iNOS, inducible nitric oxide synthase; COX-2, cyclooxygenase 2; TH, tyrosine hydroxylase; PCoA, principal coordinate analysis; GDP, guanosine diphosphate; AMP, adenosine monophosphate; GTP, guanosine triphosphate; succinyl-CoA, succinyl-coenzyme A; ADP, adenosine diphosphate; SCFA, short chain fatty acid; VIP, variable importance in projection; HRP,

horseradish peroxidase; SDH, succinate dehydrogenase; BP, biological process; CC, cellular Component; MF, molecular function.

1. Introduction

Parkinson's disease (PD) is the second most prevalent neurodegenerative disease, characterized by progressive motor symptoms, such as bradykinesia, rigidity, tremor, gait disturbance, and a wide range of non-motor symptoms, including constipation, sleep disturbances, anxiety [1]. The typical pathological manifestations of PD are progressive loss of dopaminergic neurons and the formation of Lewy bodies in the substantia nigra. Multiple risk factors have been implicated in PD, such as aging, genetic susceptibility, mitochondrial dysfunction, neuroinflammation, gut dysbiosis and energy metabolic imbalance [2]. However, the precise biological mechanisms underlying PD pathogenesis remain incompletely understood. Accumulating evidence has established impaired energy metabolism as fundamental contributors to PD pathogenesis [3]. As neurons rely heavily on oxidative phosphorylation to meet their high energy demand, disruption of energy metabolism results in insufficient adenosine triphosphate (ATP) production, excessive reactive oxygen species generation, and increased neuronal vulnerability [4]. Post-mortem analyses of PD patient brains have revealed mitochondrial abnormalities, compromised electron transport chain activity and disrupted tricarboxylic acid (TCA) cycle function [5], suggesting that metabolic reprogramming is closely associated with disease progression.

The microbiota-gut-brain axis mediates bidirectional communication between intestinal microbes and the central nervous system in PD [6]. Growing evidence demonstrates that gut commensal bacteria produce circulating bioactive metabolites that serve as regulators of mitochondrial function, TCA cycle flux and energy homeostasis. For example, dietary fiber is fermented by microorganisms to produce short chain fatty acids (SCFAs), which enter host tissues and regulate mitochondrial bioenergetics [7]. A study has validated that gut microbial perturbation could impair cerebral mitochondrial respiration and increase oxidative stress, ultimately aggravating motor dysfunction in PD animal models [8]. Also, a dedicated "microbe–mitochondrion crosstalk" has emerged as a central paradigm linking microbial ecology to bioenergetics [9]. In PD patients, metagenomic and transcriptome analyses have associated gut microbial shifts with altered microbial energy metabolism and genes involved in mitochondrial function and energy metabolism [10, 11]. Despite this framework, a critical gap persists: the specific microbial metabolite that bridges gut dysbiosis to energy metabolism failure in PD remains undefined. Elucidating these metabolic messengers will help define the microbiota-gut-brain axis and identify metabolic

guided therapeutic targets for PD.

In the present work, using α-synuclein (α-syn) (A53T) transgenic mice, we found prominent gut microbial dysbiosis that arose at the early disease stage in PD mice. Integrated omics analyses revealed the TCA cycle imbalance, and succinate, a key intermediate of the TCA cycle and important metabolite of intestinal microbiota [12], was identified as a key metabolite potentially linking gut microbial alterations and cerebral energy metabolism. Treatment of PD mice with succinate ameliorated the gut microbial dysbiosis and energy metabolism imbalance, and alleviated pathological phenotypes, including motor deficits, GI dysfunction, dopaminergic neurodegeneration, brain and gut barrier impairment. Notably, succinate also ameliorated energy metabolism imbalance associated with nucleotide metabolism in PD mice. Mechanistically, succinate exerted its neuroprotective and metabolic effects through activation of phosphoinositide 3 kinase (PI3K) / protein kinase B (Akt) / mammalian target of rapamycin (mTOR) signaling pathway. Collectively, this work revealed the potential of succinate to mediate crosstalk among gut microbial homeostasis, energy metabolism and neuronal function, providing a novel metabolic perspective for understanding the microbiota-gut-brain axis in PD and identifying promising therapeutic targets.

2. Material and methods

2.1 Animals and PD mouse model development

2.1.1 Animals

6-month-old and 12-month-old α-syn (A53T) transgenic mice and wild type (WT) mice with the same background (weighing 27-32 g) were purchased from Cavens Laboratory Animal Co., Ltd., Changzhou. Male C57BL/6J mice weighing 22-25 g were purchased from Beijing Huafukang Biological Technology Co. Ltd. Mice were kept under standard conditions (temperature 22 ± 2 ℃ and humidity 50%-60% on a 12 h light/dark cycle) in a GLP certified animal facility, where food and water were available *ad libitum*. All the experimental procedures were performed in accordance with the guidelines of the Beijing Municipal Ethics Committee for the care and use of laboratory animals, and were approved by the Animal Care & Welfare Committee, Institute of Materia Medica, CAMS&PUMC.

2.1.2 Development of rotenone-induced PD mouse model and treatments

C57BL/6J mice were randomly divided into control group, rotenone-challenged group, and rotenone + succinate (SA)-treated group. Rotenone-induced PD mice were

developed by orally administrating with freshly prepared rotenone (30 mg/kg, Sigma-Aldrich, MO, USA) suspended in 0.5% carboxymethylcellulose sodium (CMC-Na) once a day for 6 weeks. In rotenone + succinate (SA)-treated group, two weeks after orally administering rotenone, mice were simultaneously orally administrated with sodium succinate (200 mg/kg, Shanghai Aladdin Biochemical Technology Co., Ltd., China) dissolved in 0.9% NaCl once a day for 4 weeks. Control mice were orally administrated the same dose of 0.5% CMC-Na. GI functional evaluation and motor behavioral tests were performed at the end of the 6-week treatment regimen.

2.2 Motor behavior evaluations

2.2.1 Rotarod test

Rotarod test was performed as described previously [13] , using an apparatus consisting of a horizontal metal rod 50 cm long and 3 cm in diameter. Briefly, the mice were placed in the central area of the rod, and the rod was set to rotate continuously at a constant speed of 25 rpm for 120 s. The time when the mouse first fell off the rotating rod was recorded as the fall latency.

2.2.2 Pole test

The apparatus consists of a wooden pole (50 cm height, 3 cm in diameter) and a wooden ball at the top. The time taken for the mice to climb from the top to the bottom was recorded and the performance of the mice on the pole was evaluated and scored as follows: 0, falling off the pole before climbing half the distance; 1, falling off the pole after climbing half the distance; 2, sliding before climbing half the distance; 3, sliding after climbing half the distance; 4, climbing down step by step but with sliding hind limbs; 5, using four limbs and climbing down step by step in coordination [13].

2.2.3 Grip strength test

Each mouse was allowed to grasp a horizontal rope (5 mm in diameter) with its forepaws. The performance of each mouse on the rope was then scored from 0 to 5 according to the following criteria: 0, falling off the rope in 10 s; 1, gripping the rope with only 1 forepaw; 2, gripping the rope with 2 forepaws; 3, gripping the rope with 2 forepaws and only 1 hind paw; 4, gripping the rope with 2 forepaws and 2 hind paws; 5, trying to escape to the end of the rope [14].

2.2.4 Balance beam test

The balance beam (5 cm×5 cm×1 m) was placed horizontally 40 cm above the ground. Each mouse was placed at one end of the beam and allowed to walk freely across it. The time taken for the mouse to cross the balance beam and the number of falls were

recorded, and the performance was scored according to the following criteria: 0, passes the balance beam normally; 1, passes the balance beam shakily; 2, turns left and right, and unable to pass the balance beam; 3, falls off the balance beam within 60 s; 4, falls off the balance beam within 30 s; 5, falls off the balance beam within 10 s.

2.3 Gastrointestinal function evaluations

2.3.1 Fecal pellet output

Mice were fasted overnight and placed in clean empty cages without food and water, and allowed to defecate for 1 h. The number of fecal pellets were recorded, and pellets were also counted every 5 min during the first 20 min [15].

2.3.2 Whole gut transit time test

The charcoal meal suspension was prepared as follows. 20 g of gum arabic (Solarbio, Beijing, China) was accurately weighed and dissolved in 150 mL of double distilled water, and the mixture was boiled until a clear solution was formed. Subsequently, 10 g of activated charcoal powder (Fuchen, Tianjin, China) was added to the above solution, followed by three cycles of boiling. After cooling, double distilled water was supplemented to adjust the final volume to 200 mL. The suspension was stored at 4 °C and thoroughly shaken prior to use. Mice were administered the charcoal suspension (20 mL/kg) via intragastric perfusion and then housed in clean empty cages. The time interval from gavage to the first observation of black fecal pellets was recorded [16].

2.3.3 Fecal water content

Mice were placed in clean empty cages and allowed to defecate for 1 h. Fresh fecal samples were collected into centrifuge tubes immediately after excretion. The wet weight of each fecal sample was recorded, and then dried at 65 °C for 24 h. Subsequently, the dry weight was determined. Fecal water content was calculated according to the following formula: [(wet weight − dry weight)/wet weight] × 100% [16].

2.4 Immunohistochemistry staining

Mouse midbrain was isolated, fixed in 4% paraformaldehyde, and then subjected to gradient dehydration, paraffin embedding, and continuous coronal sectioning. For immunohistochemical staining, paraffin sections were deparaffinized and rehydrated, and antigen retrieval was performed. After incubation with 3% H_2O_2 (ANNJET, China) for 25 min to block endogenous peroxidase activity, sections were sealed with 3% bovine serum albumin (Servicebio, China) for 30 min at room temperature. Subsequently, Sections were incubated with tyrosine hydroxylase (TH) (Servicebio,

China) followed by secondary antibody conjugated with streptavidin-labeled peroxidase (Servicebio, China). Finally, the labeling was visualized with 3,3′-diaminobenzidine (Servicebio, China) and the images were captured by light microscope (Nikon E600, Japan).

2.5 16S rRNA gene sequencing

Total genomic DNA from stool samples were extracted using the CTAB/SDS method. DNA concentration and purity were monitored on 1% agarose gels, and the DNA sample was diluted to 1 ng/μL with sterile water. Variable regions of the 16S rRNA gene were amplified using barcoded specific primers. All PCR reactions were performed in a system containing 15 μL of Phusion® High Fidelity PCR Master Mix (New England Biolabs), 0.2 μM of forward and reverse primers, and 10 ng template DNA. Equal volumes of PCR products and 1× loading buffer were mixed, and the mixture was separated on a 2% agarose gel. Target PCR fragments were then purified using the Qiagen Gel Extraction Kit (Qiagen, Germany). Sequencing libraries were constructed with the TruSeq® DNA PCR Free Sample Preparation Kit (Illumina, USA) according to the manufacturer's instructions, and index codes were incorporated. Library quality was validated using a Qubit@ 2.0 Fluorometer (Thermo Scientific) and the Agilent Bioanalyzer 2100 system. Qualified libraries were sequenced on the Illumina NovaSeq platform to generate 250 bp paired end reads. Raw sequencing reads were quality filtered using fastp to obtain high-quality clean tags. Paired end reads were merged via FLASH software, and chimeric sequences were identified and removed using the UCHIME algorithm. Clean valid tags were finally obtained for subsequent microbial community analysis.

2.6 Proteomics analysis

Mouse midbrain was fully homogenized in cold RIPA lysis buffer (Sangon Biotech, China) containing protease and phosphatase inhibitors. The homogenate was centrifuged (12,000 rpm, 4 °C, 30 min) and the total protein concentration in the supernant was quantified using a BCA protein assay kit (Yeasen, China). Aliquots (25 μg total protein) were denatured with 100 μL 50 mM NH_4HCO_3 and 100 μL 100 mM DTT (Sigma-Aldrich, USA) (prepared in 8 M urea) at 56 °C for 30 min. Samples were transferred to 10 kDa ultrafiltration devices, centrifuged (14,000 × g, 4 °C, 20 min), and washed twice with 50 mM NH_4HCO_3. Proteins were alkylated with 150 μL 20 mM IAA (prepared with 50 mM NH_4HCO_3) in the dark for 30 min, followed by two additional washes with NH_4HCO_3. Trypsin was added for overnight digestion at 37 °C

(600 rpm). Peptides were collected by centrifugation, desalted with double distilled water, and lyophilized. The digested peptides were desalted using C18 resin (Millipore, USA). For LC-MS/MS analysis, peptides were resuspended in 10 μL waters, centrifuged (15,000 × g, 4 °C, 20 min), and 8 μL supernatant was loaded. Separation was performed on an UltiMate 3000 UHPLC coupled to an Orbitrap Fusion Lumos Tribrid mass spectrometer. Raw data were processed using Proteome Discoverer 2.3 (Thermo Fisher Scientific) with SEQUEST HT for peptide identification. Differentially expressed proteins ($p < 0.05$, fold change ≥ 1.5) were analyzed via Kyoto Encyclopedia of Genes and Genomes (KEGG) pathway enrichment using Apexbio's pipeline.

2.7 Metabolomics analysis

For serum samples, 50 μL of serum was mixed with 250 μL of 20% acetonitrile/methanol solution, vortexed for 3 min, and centrifuged (12,000 rpm, 4 °C, 10 min). A total of 250 μL supernatant was collected, incubated at −20 °C for 30 min, and re-centrifuged under identical conditions. Finally, 180 μL of the supernatant was filtered through a protein precipitation plate for subsequent LC-MS analysis. For midbrain samples, 50 mg of sample was mixed with 500 μL of 70% methanol/water solution. The mixture was vortexed at 2500 rpm for 3 min and centrifuged (12,000 rpm, 4 °C, 10 min). A 300 μL aliquot of the supernatant was transferred into a new centrifuge tube and incubated at −20 °C for 30 min, followed by a second centrifugation (12,000 rpm, 4 °C, 10 min). Finally, 200 μL of the resulting supernatant was loaded onto a protein precipitation plate for subsequent LC-MS analysis. Sample extracts were analyzed on an LC-ESI-MS/MS platform consisting of a Waters ACQUITY H-Class UHPLC system coupled to a QTRAP® 6500+ mass spectrometer. For the amide separation method, chromatographic separation was performed using an ACQUITY UPLC BEH Amide column (2.1 mm × 100 mm, 1.7 μm). Mobile phase A consisted of water containing 10 mM ammonium acetate and 0.3% ammonium hydroxide, and mobile phase B was 90% acetonitrile water. The elution gradient was programmed as follows: initial 95% B (0–1.2 min), reduced to 70% B at 8 min, held at 50% B from 9 to 11 min, and returned to 95% B for re-equilibration (11.1–15 min). The flow rate was set at 0.4 mL/min. The column temperature was maintained at 40 °C, and the injection volume was 2 μL. Differentially regulated metabolites were screened based on variable importance in projection (VIP) values and the absolute log_2FC. Metabolite annotation was performed against the KEGG compound database, and annotated metabolites were further assigned to corresponding KEGG pathways.

2.8 Transcriptome analysis

Total RNA was extracted using the phenol guanidine isothiocyanate method and dissolved in DEPC water. RNA concentration was accurately quantified using a Qubit fluorometer. For mRNA library construction, poly(A) tailed mRNA was enriched via Oligo(dT) magnetic beads and fragmented into short fragments with fragmentation buffer. First strand cDNA was synthesized by reverse transcription with random hexamer primers, followed by second strand cDNA synthesis, end repair, and dA-Tailing. Sequencing adapters were ligated to the cDNA fragments. After magnetic bead purification and fragment selection, libraries with insert sizes of 250–350 bp were obtained. Adapter ligated products were amplified by PCR and purified again with DNA magnetic beads, and the final library was eluted in nuclease free water. Library quality was assessed by Qubit quantification and fragment size detection using a Qsep400 analyzer. Qualified libraries were pooled according to their effective concentration and target sequencing depth, then sequenced on the Illumina platform to generate 150 bp paired-end reads. Raw reads were quality trimmed with fastp to remove adapter containing sequences. Gene expression was quantified using feature Counts, and FPKM values were calculated for transcript normalization based on gene length. Differential expression analysis between groups was performed using DESeq2. Functional enrichment for Gene Ontology (GO) terms and KEGG pathways was carried out using hypergeometric tests.

2.9 Succinate content detection

Succinate content was measured by the Amplex Red Succinic Acid Assay Kit (Beyotime Biotechnology Co., Ltd., China). All the experimental procedures were performed following the instructions recommended by the manufacturer. Briefly, every 10 mg of tissue was added to 100 μL of BeyoLysis™ Buffer A. After the tissue was ground thoroughly, it was centrifuged (12,000 × g, 4 ºC, 5 min), and the supernatant was collected for subsequent detection. The Amplex Red working solution was prepared according to the instructions. The content was determined using fluorescence detection. A standard curve was established using succinate standards. The mass concentration of succinate in the sample was calculated based on the molecular weight of 118.

2.10 Western blot

The midbrain and colon were homogenized and lysed with RIPA buffer (Sangon Biotech, China) containing protease inhibitor and phosphatase inhibitor. Protein quantification was performed by the BCA assay kit according to the manufacturer's standardized protocol. Protein samples were resolved via 8% and 10% SDS-PAGE (Yeasen, China) and transferred onto PVDF membranes (Merck Millipore, Germany). Membranes were blocked with 5% BSA for 2 h at room temperature and subsequently incubated overnight at 4 °C with the following primary antibodies: inducible-nitric oxide synthase (iNOS) (1:1000, Abcam, ab15323), cyclooxygenase 2 (COX-2) (1:1000, Abcam, ab15191), TH (1:1000, ABclonal, A0028), Occludin (1:5000, abmart, TB2814), Claudin-1 (1:1000, abmart, PA2349), p-PI3K (1:2000, abmart, T40116F), PI3K (1:2000, abmart, T40115F), p-Akt (1:500, ABclonal, AP1208), Akt (1:1000, ABclonal, A11016), p-mTOR (1:1000, abmart, T56571), mTOR (1:1000, abmart, T55306), β-actin (1:50000, ABclonal, AC026), GAPDH (1:50000, ABclonal, A19056). The membrane was washed and incubated with following horseradish peroxidase (HRP)-conjugated secondary antibodies: anti-mouse IgG (1:2000, Abclonal, AS071) and anti-rabbit IgG (1:2000, Abclonal, AS014) for 2 h. The density of the bands was imaged using a Super ECL Detection Reagent kit (Yeasen, China) and LAS 4000 chemiluminescence system (GE, USA). Gel-pro analyzer 3.2 was used to analyze the intensities of bands. The intensity of each target band was normalized to the loading control (GAPDH or β-actin) from the same lane.

2.11 Statistical analysis

All data was expressed as means ± SEM and analyzed using GraphPad Prism 10.1.2 software. Student's t-tests were used when comparing two groups and one-way ANOVA was used for comparisons among three or more groups. Values with $P < 0.05$ were considered statistically significant.

3. Results

3.1 Microbiota-gut-brain axis disturbed in α-syn (A53T) transgenic mice

To characterize the progressive PD-like pathological and behavioral phenotypes of α-syn (A53T) transgenic mice at different disease stages, we performed behavioral tests and dopaminergic neuron evaluation. Behavioral assessments revealed no obvious motor dysfunction in 6-month-old α-syn (A53T) mice, whereas significant motor

impairments were evident in 12-month-old mice, as validated by the pole test, grip strength test (Figure 1A, B) and rotarod test, balance beam test (Figure S1A-C). The number of TH-positive neurons were also consistently reduced (Figure 1C, D). GI function assessment revealed that 6-month-old α-syn (A53T) mice showed fewer stool pellets and prolonged whole gut transit time, while fecal water content was not significantly altered. These deficits progressed with age and became more severe at 12 months (Figure 1E-I). These results demonstrated that GI abnormalities represent an early event in PD progression.

To characterize dynamic gut-microbiome remodeling throughout PD progression, we then performed 16S rRNA sequencing on fecal samples. In 6-month-old α-syn (A53T) mice, the gut microbiota composition underwent significant alterations (Figure S1D), with decreased richness and evenness from alpha diversity analysis (Figure S1E, F) and a distinct separation of microbial communities between groups from beta diversity analysis (Figure S1G, H). Taxonomic profiling further confirmed obvious compositional differences in gut microbiota between groups at 6 months of age, such as reduced abundance of *Bacteroidetes* and enrichment of *Firmicutes* at the phylum level (Figure S1I) and reduced abundance of *Bacteroidales* at the order level (Figure S1J). These microbial communities are closely related to energy metabolism [11,17,18]. 12-month-old α-syn (A53T) mice displayed more severe gut microbiota dysbiosis (Figure 1J), as shown by alpha diversity analysis (Figure 1K, L) and beta diversity analysis (Figure 1M, N). Taxonomic comparison further revealed that more profound gut microbiota compositional changes in 12-month-old mice, including reduced abundance of *Firmicutes* and *Bacteroidota* at the phylum level, and *Bacteroidales* at the order level (Figure 1O, P). These microbial shifts were not only closely related to the supply of energy producing metabolites, but also indicated disrupted microbial homeostasis, as reflected by increased *Proteobacteria* abundance [17, 18]. These results demonstrated that α-syn (A53T) mice exhibited early PD-associated GI dysfunction and gut microbiota dysbiosis, and these altered gut bacteria, largely linked to energy metabolism, may serve as an important contributor to energy metabolic disturbances underlying PD pathogenesis.

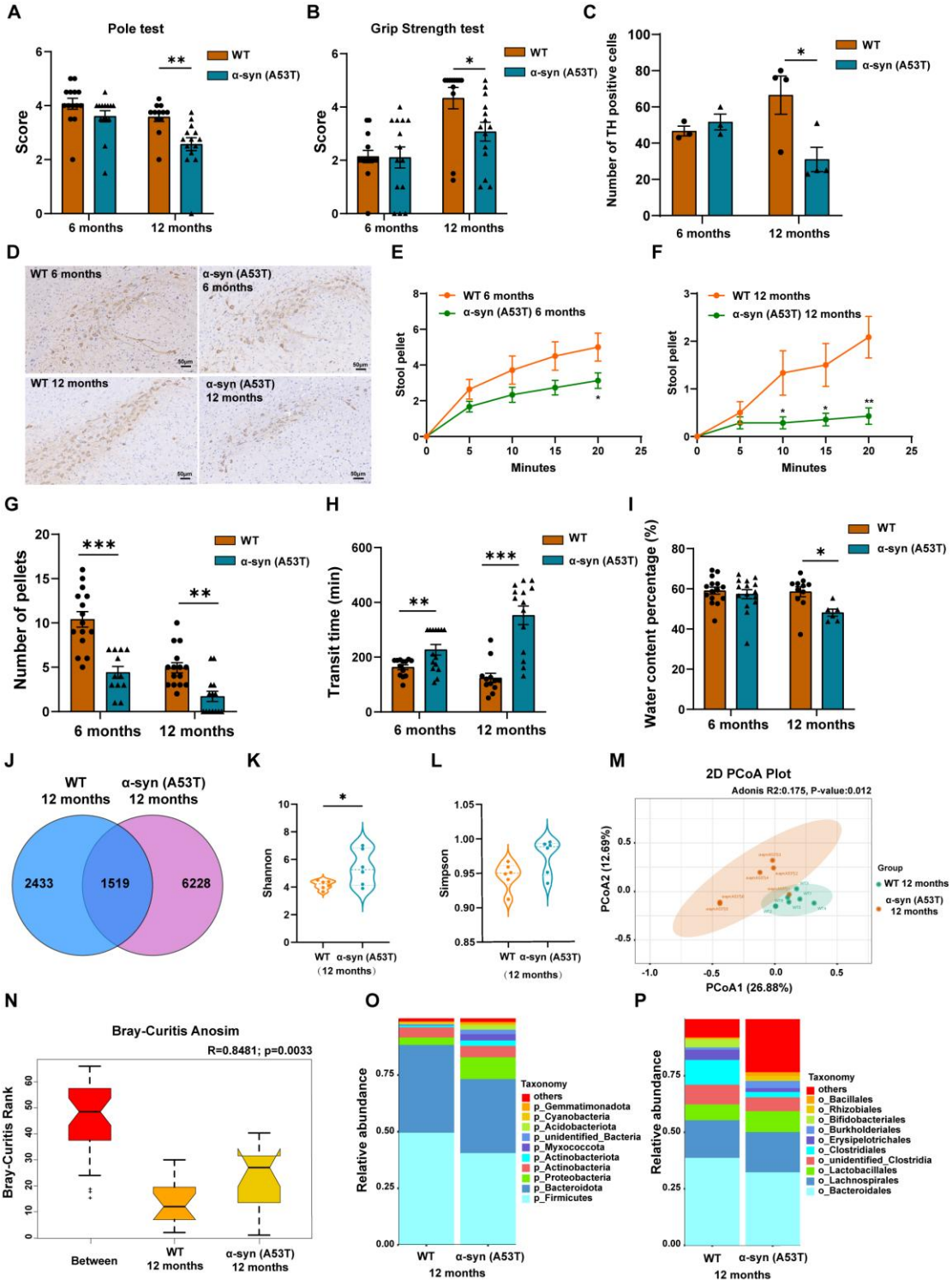


Figure 1. PD mice exhibited motor and gastrointestinal dysfunction, accompanied by gut microbiota dysbiosis. Behavioral tests and gastrointestinal function tests were conducted on 6-month-old and 12-month-old α-syn (A53T) mice. (A) Pole test performance score; (B) Grip strength test performance score. n = 12-14 mice per group. (C) Quantification of TH-positive cells; (D) Immunohistochemistry of TH staining in the substantia nigra. n = 3-4 mice per group. (E) Fecal output over 20 min in 6-month-

old α-syn (A53T) mice; (F) Fecal output in 20 min in 12-month-old α-syn (A53T) mice; (G) Number of fecal pellets output in 1 h; (H) Whole gut transit time; (I) Fecal water content percentage. n = 6-15 mice per group. Fecal samples were collected from 12-month-old α-syn (A53T) mice for 16S rRNA gene sequencing. (J) Venn diagram based on ASVs for WT group and α-syn (A53T) group; (K) Alpha diversity analysis of gut microbiota based on Shannon index; (L) Alpha diversity analysis of gut microbiota based on Simpson index; (M) Beta diversity analysis based on PCoA; (N) Beta diversity analysis among different groups based on ANOSIM; (O) Taxonomic profiling of gut microbiota at the phylum level; (P) Taxonomic profiling of gut microbiota at the order level. n = 6 mice per group. Data are presented as means ± SEM. $^{*}P < 0.05$, $^{**}P < 0.01$, $^{***}P < 0.001$ *versus* WT mice.

3.2 Multi-omics analyses revealed perturbated TCA cycle and decreased succinate in PD mice

We next integrated multi-omics analyses to identify potential mechanisms of metabolic disturbances in 12-month-old α-syn (A53T) mice. Proteomic analysis identified 94 differentially expressed proteins, including 31 upregulated and 63 downregulated proteins in the midbrain of α-syn (A53T) mice compared with WT mice (Figure 2A). KEGG pathway enrichment analysis revealed that these proteins were predominantly enriched in pyruvate metabolism, TCA cycle, and carbon metabolism (Figure 2B). Consistently, PICRUSt functional prediction based on 16S rRNA sequencing of 12-month-old α-syn (A53T) mice indicated that the altered gut microbiota was mainly enriched in carbohydrate metabolism, amino acid metabolism, metabolism of cofactors and vitamins, as well as energy metabolism pathways (Figure 2C). In addition, targeted metabolomics analysis in serum revealed that multiple metabolites in TCA cycle were significantly reduced in α-syn (A53T) mice, including succinate, α-ketoglutarate, and malate (Figure 2D-F), whereas citrate, isocitrate, and pyruvate exhibited decreased trends without statistical significance (Figure S2A-D). Correlation analysis performed between TCA cycle intermediates and motor behavioral parameters revealed that succinate showed the strongest correlations among the detected metabolites (Figure S2E). Succinate was also found to be decreased in the midbrain of α-syn (A53T) mice (Figure 2G), suggesting that succinate may serve as a key metabolite involved in TCA cycle impairment. 16S rRNA sequencing further revealed that multiple succinate producing taxa were reduced across various taxonomic levels, such as members of *Bacteroidota* (*Bacteroidota, Bacteroidia,*

Bacteroidales)[19-21], *Verrucomicrobiota* (*Verrucomicrobiota, Verrucomicrobiae, Verrucomicrobiales, Akkermansiaceae*)[22-25], and *Desulfobacterota* (*Desulfovibrionia, Desulfovibrionales*) [26, 27] (Figure S2F-I). Together with the omics findings, these results further supported succinate as a key metabolite linking gut microbiota dysbiosis to TCA cycle dysfunction in PD progression.

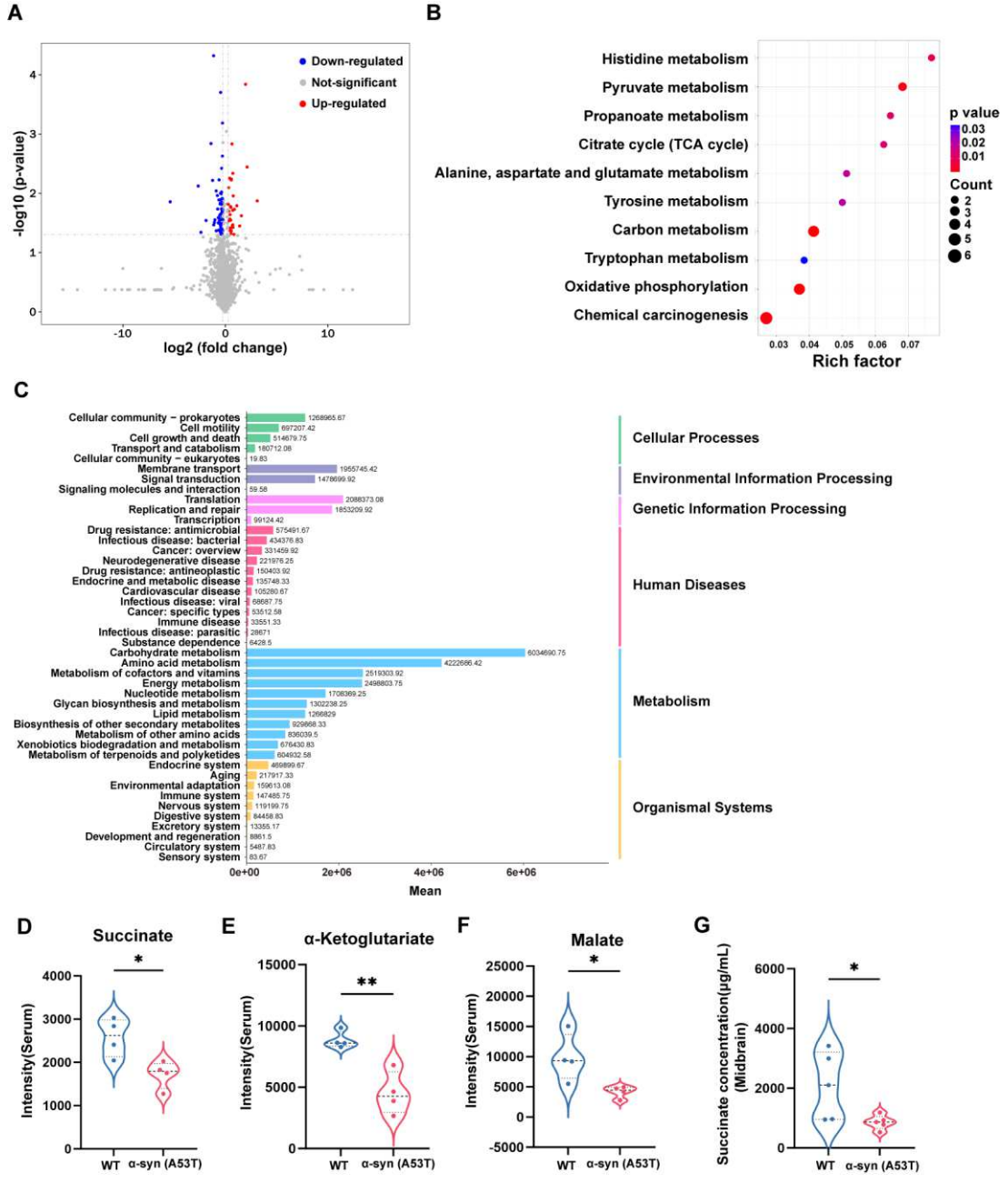


Figure 2. α-syn (A53T) mice displayed perturbed TCA cycle homeostasis and reduced succinate levels. Midbrains were collected from 12-month-old α-syn (A53T) mice for proteomic analysis. (A) Volcano plot of differentially expressed proteins; (B) KEGG pathway enrichment analysis. n = 3 per group. Fecal samples were collected from 12-month-old α-syn (A53T) mice for 16S rRNA gene sequencing. (C) PICRUSt-

based prediction of KEGG functional pathways. Serum was collected from 12-month-old α-syn (A53T) mice for targeted metabolomic analysis. (D-F) Levels of succinate, α-ketoglutarate and malate in the serum. n = 4 mice per group. (G) Succinate concentration in the midbrain. n = 5 mice per group. Data are presented as means ± SEM. $^{*}P < 0.05$, $^{**}P < 0.01$ *versus* WT mice.

3.3 Succinate alleviated motor and gastrointestinal deficits in PD mice

To investigate the effects of the differential metabolite succinate on PD pathology, we performed validation experiments using rotenone-induced PD mice. Behavioral tests demonstrated that succinate significantly ameliorated motor deficits in rotenone-induced PD mice. Specifically, compared with rotenone-challenged mice, succinate treatment prolonged the latency for mice to fall in the rotarod test (Figure 3A), improved performance in the balance beam test, as measured by foot slip number, traversal time and performance score (Figure 3B), as well as in the pole and grip strength tests (Figure 3C, D). GI function results showed that succinate significantly increased the fecal frequency, stool pellet output and fecal water content compared with rotenone mice (Figure 3E-G). TH expression was examined by immunohistochemistry and Western blot analysis. Succinate treatment increased the number of TH-positive neurons in the substantia nigra (Figure 3H) and restored TH protein expression in both midbrain and colon (Figure 3I, J), suggesting the attenuation of dopaminergic neuronal injury. Moreover, succinate treatment improved brain and colon barrier function by increasing the expression of claudin-1 and occludin (Figure 3K-N). We also found that succinate significantly inhibited NO production and the expression of iNOS and COX-2 in BV2 cells, midbrain and colon of PD mice (Figure S3A-H). These findings revealed that succinate could alleviate motor and intestine deficits as well as the pathological changes in rotenone-induced PD mice.

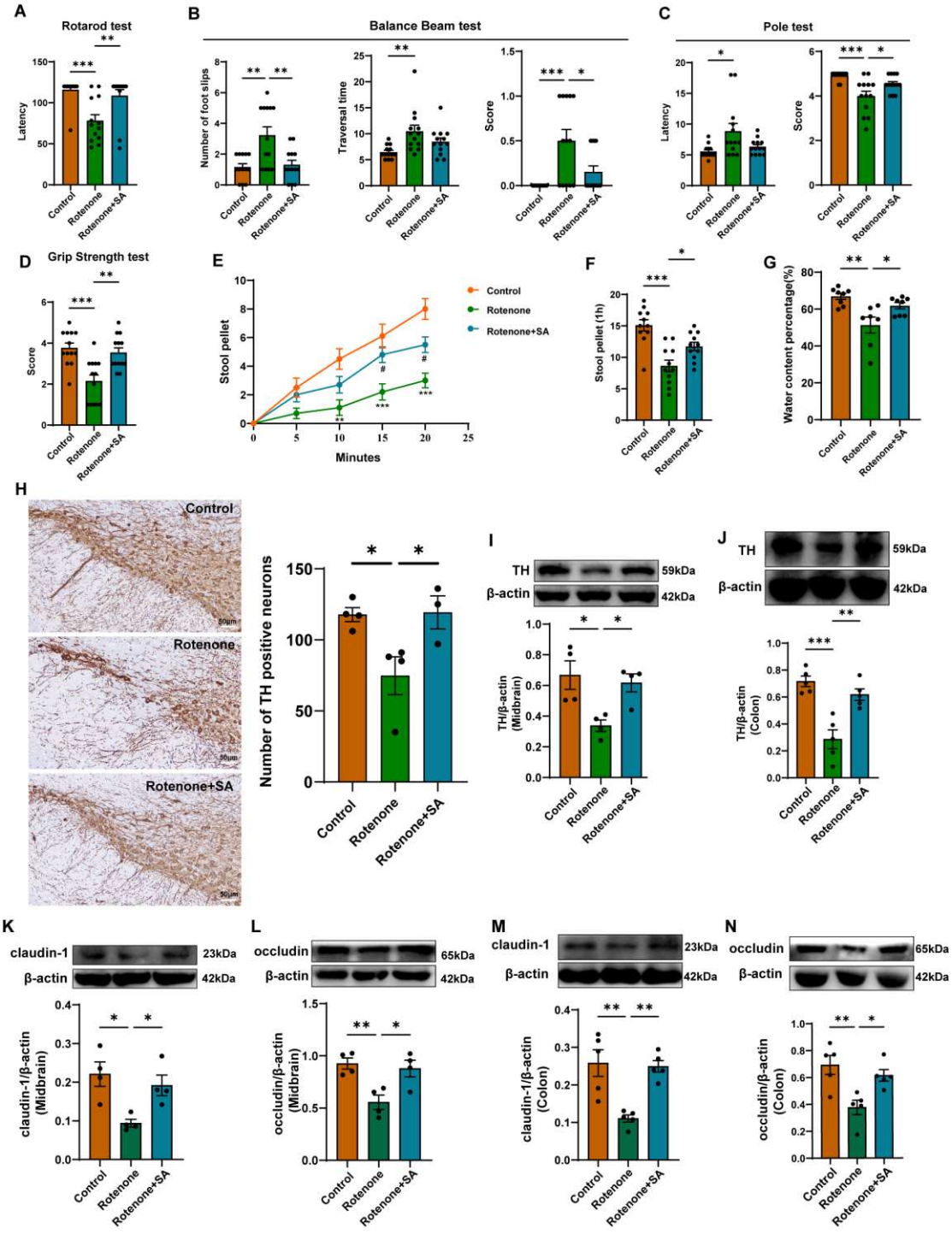


Figure 3. Succinate alleviated motor and gastrointestinal deficits in PD mice. Rotenone-induced PD mice were orally administered succinate (200 mg/kg) once daily for 4 consecutive weeks. (A) Latency on the rotarod; (B) Number of foot slips, transversal time and performance score of balance beam test; (C) Latency and performance score of pole test; (D) Grip strength test performance score; n = 13 mice per group. (E) Fecal output over 20 min; (F) Number of fecal pellets produced in 1 h; (G) Fecal water content; n = 7-11 mice per group. (H) Quantification of TH-positive

neurons from immunohistochemical staining; (I) Western blot analysis of TH expression in the midbrain. n = 3-4 mice per group. (J) Western blot analysis of TH expression in the colon; (K) Western blot analysis of claudin-1 expression in the midbrain; (L) Western blot analysis of occludin expression in the midbrain; (M) Western blot analysis of claudin-1 expression in the colon; (N) Western blot analysis of occludin expression in the colon. n = 4-5 mice per group. Data are presented as means ± SEM. $^{*}P < 0.05$, $^{**}P < 0.01$, $^{***}P < 0.001$.

3.4 Succinate ameliorated gut microbiota dysbiosis in rotenone-induced PD mice

To determine the impact of succinate on gut microbiota, fecal samples from control, rotenone and succinate-treated mice were subjected to 16S rRNA gene sequencing. A total of 383 ASVs were present in all three groups, representing the core shared gut microbial taxa among the mice (Figure 4A). Alpha diversity analysis revealed that rotenone significantly increased the richness and evenness of the gut microbiota, whereas succinate treatment failed to reverse this elevation (Figure 4B, C). However, beta diversity analysis showed that the microbial community was distinct across the three groups (Figure 4D, E), indicating that succinate intervention substantially remodeled the overall structure of the rotenone-perturbed gut microbiota. We next analyzed the taxonomic composition of the gut microbiota following succinate treatment. Rotenone changed the relative abundance of bacterial taxa such as reduced *Bacteroidota*, enrichment of *Firmicutes* and *Lachnospirales*, while succinate treatment shifted their distribution closer to that of the control group (Figure 4F, G). Additionally, various succinate-related bacterial taxa showed decreasing trends in the rotenone group, and succinate treatment partially restored their abundance and altered the distribution of intestinal flora, such as members of *Bacteroidota* (*Bacteroidota, Bacteroidia, Bacteroidales*), *Verrucomicrobiota* (*Verrucomicrobiota, Verrucomicrobiae, Verrucomicrobiales, Akkermansiaceae*), and *Desulfobacterota* (*Desulfovibrionia, Desulfovibrionales*) (Figure S4A-D). These findings demonstrated that succinate remodeled the gut microbial diversity, abundance of bacterial taxa, and gut community structure in PD mice.

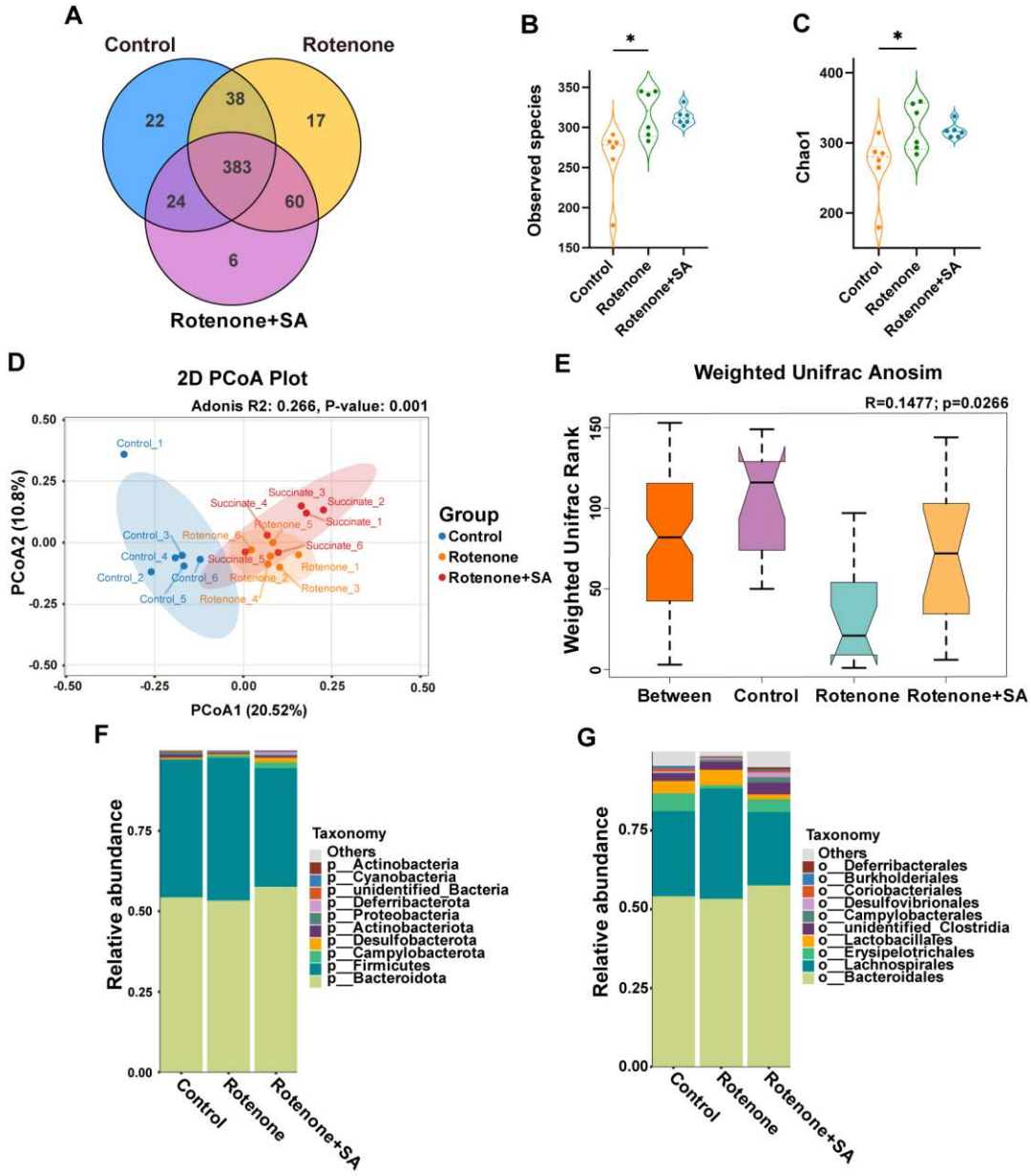


Figure 4. Succinate ameliorated gut microbiota dysbiosis in rotenone-induced PD mice. Fecal samples were collected from rotenone-induced PD mice for 16S rRNA gene sequencing. (A) Venn diagram based on ASVs; (B) Alpha diversity analysis of gut microbiota based on observed species; (C) Alpha diversity analysis of gut microbiota based on Chao1; (D) Beta diversity analysis based on PCoA; (E) Beta diversity analysis among different groups based on ANOSIM; (F) Taxonomic profiling of gut microbiota at the phylum level; (G) Taxonomic profiling of gut microbiota at the order level. n = 6 per group. Data are presented as means ± SEM. $^{*}P < 0.05$.

3.5 Succinate improved energy metabolism in rotenone-induced PD mice

We further employed metabolomics to assess midbrain energy metabolism alterations following rotenone exposure and the therapeutic effect of succinate

intervention. Rotenone elicited changes in TCA cycle intermediates, reducing succinate and pyruvate while increasing malate and isocitrate. Succinate supplementation partially rescued these metabolic shifts, though no consistent significant changes were observed for the TCA metabolite pool (Table S1). By contrast, purine nucleotide metabolites were substantially altered in rotenone-challenged mice, with guanosine diphosphate (GDP) and adenosine monophosphate (AMP) significantly upregulated, and succinate treatment reduced these two metabolites (Figure 5A, D). In addition, rotenone stimulation markedly decreased the guanosine triphosphate (GTP)/GDP ratio, whereas succinate treatment increased this ratio (Figure 5B). Similarly, the ATP/AMP ratio exhibited a decreasing trend in the rotenone group, and increased after succinate intervention (Figure 5D). Rotenone stimulation induced a rising trend in both GTP and ATP levels, which was partially reversed by succinate supplementation, although these alterations did not reach statistical significance (Figure 5C, F). Together, our metabolomic results show that succinate reverses rotenone-mediated disturbances in purine nucleotide metabolism and recovers phosphorylation ratios to relieve mitochondrial energy stress, even though no marked elevations of ATP and GTP were observed.

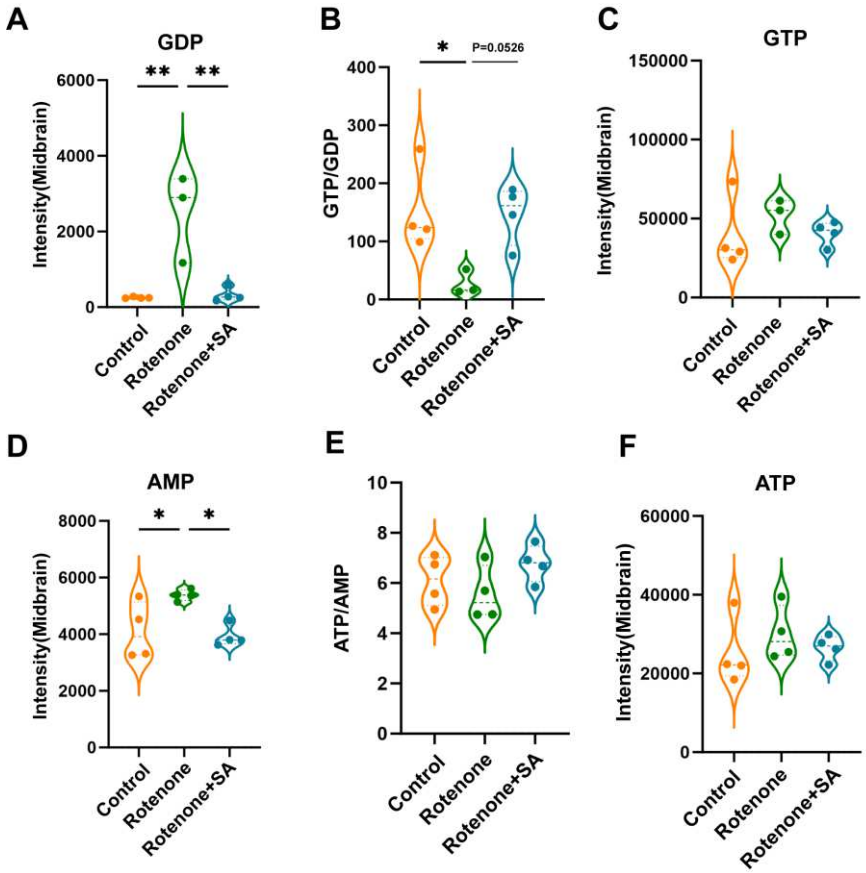


Figure 5. Succinate improved energy metabolism in rotenone-induced PD mice. Rotenone-induced PD mice were orally administered succinate (200 mg/kg) once daily for 4 consecutive weeks, and the midbrain samples were collected for metabolomics. (A) GDP intensity; (B) GTP/GDP ratio; (C) GTP intensity; (D) AMP intensity; (E) ATP/AMP ratio; (F) ATP intensity. n = 3-4 per group. Data are presented as means ± SEM. $^{*}P < 0.05$, $^{**}P < 0.01$.

3.6 Succinate alleviated PD pathology through activating PI3K/Akt/mTOR pathway

We then performed transcriptomic analysis to explore the molecular mechanisms by which succinate alleviated PD pathology. Venn diagram uncovered 68 overlapping differentially expressed genes between the Rotenone vs. Control and Rotenone + SA vs. Rotenone comparisons in the midbrain (Figure 6A). GO enrichment analysis indicated that these genes were mainly enriched in metabolic processes within the biological process category (Figure 6B). KEGG pathway analysis further highlighted significant enrichment of the PI3K/Akt signaling pathway among the top ranked pathways for both comparisons (Figure 6C, D), implying that PI3K/Akt might mediate succinate-dependent metabolic process. Since PI3K/Akt/mTOR signaling pathway plays a vital role in regulating cellular energy metabolism [28], we further assessed its activation in the midbrain and colon. The results showed that rotenone substantially decreased PI3K, Akt and mTOR phosphorylation in both midbrain and colon of PD mice, and succinate treatment significantly restored these phosphorylation events, re-activating this pathway in PD mice (Figure 6E-L). Collectively, these data suggested that succinate ameliorated energy metabolism and PD pathology by activating PI3K/Akt/mTOR signaling.

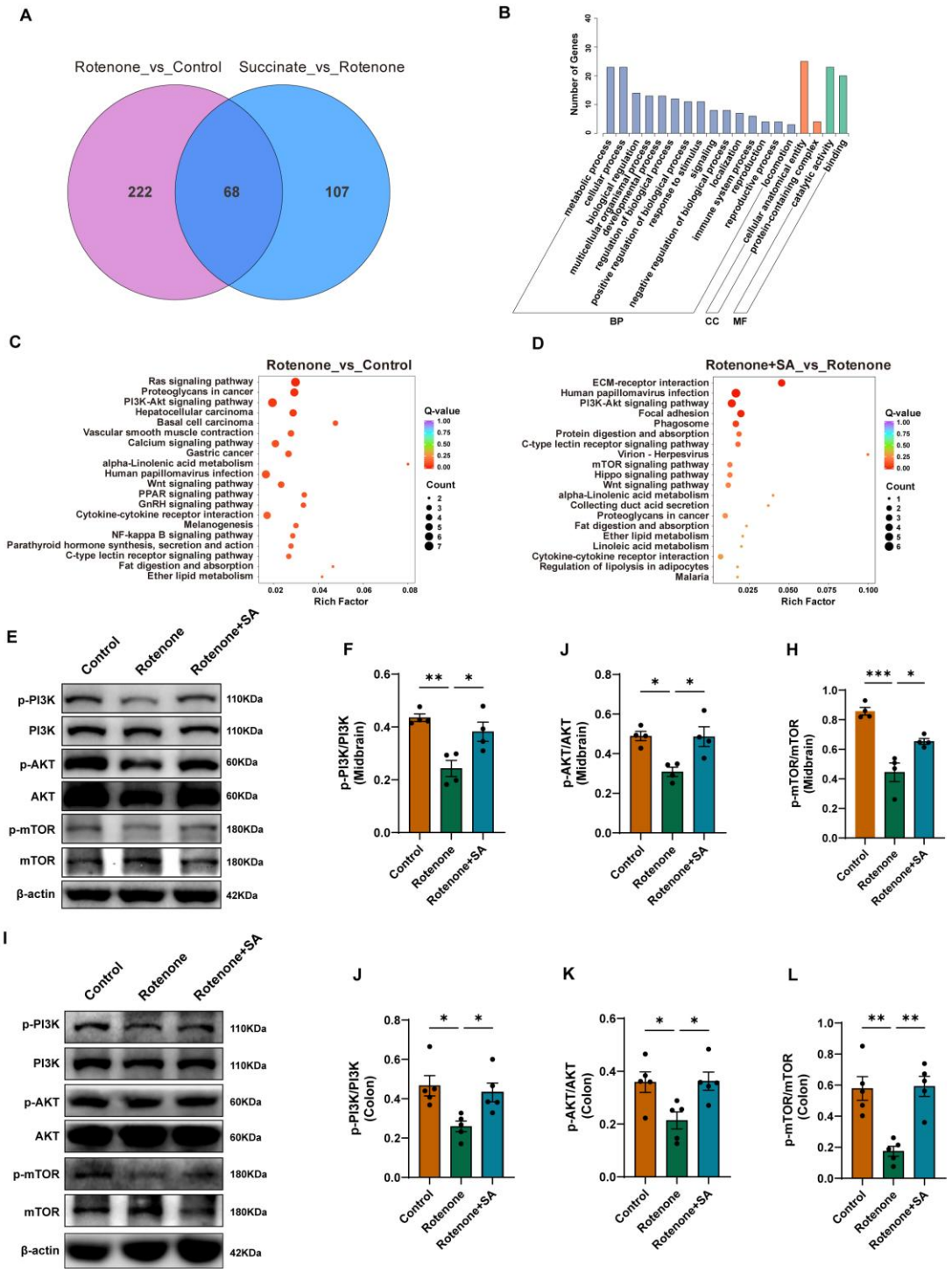


Figure 6. Succinate alleviated PD pathology through activating PI3K/Akt/mTOR pathway. Rotenone-induced PD mice were orally administered succinate (200 mg/kg) once daily for 4 consecutive weeks, and the midbrains were collected for transcriptomic analysis. (A) Venn diagram of differentially expressed genes; (B) GO enrichment analysis based on differentially expressed genes; (C) The top 20 enriched KEGG terms for differentially expressed genes in "Rotenone vs Control"; (D) The top 20 enriched KEGG terms for differentially expressed genes in "Rotenone + SA vs Rotenone". n =

3 mice per group. (E-H) Western blot analysis of p-PI3K, PI3K, p-Akt, Akt, p-mTOR and mTOR expression in the midbrain; (I-J) Western blot analysis of p-PI3K, PI3K, p-Akt, Akt, p-mTOR and mTOR expression in the colon. n = 4-5 mice per group. Data are presented as means ± SEM. $^{*}P < 0.05$, $^{**}P < 0.01$, $^{***}P < 0.001$.

4. Discussion

Increasing evidence has long recognized that GI dysfunction precedes the classical motor symptoms of PD by decades, supporting the concept that PD pathology may originate in the gut and spread to the brain via the vagal nerve [29]. In parallel, gut microbial dysbiosis has been consistently identified in PD patients and multiple animal models, although the altered bacterial taxa vary across studies [30, 31]. Our results also revealed that GI dysfunction and gut microbiota dysbiosis occurred in 6-month-old α-syn (A53T) mice, prior to dopaminergic neuronal loss and motor deficits, confirming gut disturbances as an early event in PD pathological cascade. In contrast, 12-month-old α-syn (A53T) mice developed severe motor impairments, accompanied by further deterioration of microbial community disorder. Notably, the alpha diversity of the gut microbiota decreased in 6-month-old α-syn (A53T) mice, but increased in 12-month-old mice. This age-dependent shift demonstrated that the gut microbiota dysbiosis in α-syn (A53T) mice did not simply manifest as uniformly reduced diversity; instead, it evolved from early stage diversity impairment to extensive community structure remodeling with disease progression, consistent with age dependent microbial dynamics reported previously [32].

Commensal bacteria influence systemic and cerebral energy homeostasis via microbe-derived metabolites [33, 34]. Fermentation products of gut microbiota including SCFAs, and other organic acids serve as bioactive signaling molecules and TCA cycle substrates that modulate mitochondrial bioenergetics in peripheral tissues and neurons[35-37]. In this work, we found reduced abundance of *Firmicutes* and *Bacteroidota*, alongside enrichment of *Proteobacteria* at the phylum level in 12-month-old α-syn (A53T) mice. *Bacteroides* are closely associated with the production of key carbon substrates that drive energy metabolism, such as acetate, propionate, and succinate [38]. *Firmicutes* encompassing functionally heterogeneous taxa can provide substrates for oxidative phosphorylation, while also including pathogenic bacteria capable of altering intestinal carbon flux [11, 39]. These results suggested that α-Syn (A53T) mice may have already experienced a decline in intestinal metabolic function in the early stages, and impaired peripheral metabolite supply. Also, the continued

reduction in the main producers of key carbon substrates may further decrease the supply of energy producing metabolites [17]. Besides, we observed that certain bacterial taxa exhibited opposite trends along disease progression. For instance, the relative abundance of *Firmicutes* was elevated in 6-month-old α-syn (A53T) mice, whereas this taxon declined in 12-month-old mice. Such divergent microbial responses may arise from the distinct gut and systemic microenvironments between presymptomatic and advanced disease stages. Cross-sectional microbiome profiling based on single time-point sampling may fail to capture these dynamic shifts, which may lead to biased interpretation of PD-associated gut dysbiosis [40]. Nevertheless, this stage-dependent microbial shifts further support the notion that gut microbiota dysbiosis undergoes dynamic remodeling rather than unidirectional alteration during the progression of PD [41]. Furthermore, multi-omics analysis revealed TCA cycle dysregulation in PD mice, and this metabolic disturbance was associated with gut microbiota dysbiosis. Several bacterial taxa exhibiting altered abundance, such as *Bacteroidetes*, *Firmicutes* and *Proteobacteria*, were closely associated with energy metabolism. Meanwhile, succinate was identified as a differentially abundant metabolite and was detected changes in multiple succinate-producing gut bacterial taxa, such as *Bacteroidota*, *Verrucomicrobiae* and *Akkermansiaceae*. These findings further suggested that succinate acted as a key metabolite bridging gut dysbiosis and impaired energy metabolism.

Succinate, a key TCA cycle intermediate and gut microbial metabolite, originates from both host mitochondrial metabolism and intestinal microbial fermentation[12]. Aberrant succinate metabolism is tightly involved in mitochondrial dysfunction, redox imbalance, and superoxide production [42]. Notably, current studies on the role of succinate in PD pathogenesis remain controversial. On one hand, gut microbiota-produced succinate was reported to aggravate α-syn aggregation, disrupted protein homeostasis, and promoted dopaminergic neurodegeneration [43]. On the other hand, succinate treatment effectively rescued energy depletion and restored reduced dopamine levels of rats caused by succinate dehydrogenase (SDH) inhibition [44]. Consistent with this protective effects, combined action of panthenol and succinate alleviated rotenone-induced oxidative stress, improved cerebral redox homeostasis, and exerted neuroprotective effects in PD mice [45]. These divergent observations suggested that the biological effects of succinate were condition-specific, possibly determined by its source, concentration and experimental models. Our findings

supported the potential neuroprotective effects of exogenous succinate. In rotenone-reduced PD mice, succinate partially alleviated gut microbial dysbiosis and mitigated energy metabolic imbalance, accompanied by improved GI function, motor behavior. Succinate couples TCA cycle turnover with mitochondrial electron transport. Beyond its canonical function in driving ATP production, succinate also acts as a bioactive metabolic messenger to regulate cellular metabolic reprogramming [42]. Purine nucleotides (GDP, GTP, AMP, ADP) serve as stable indicators of cellular energy status, with AMP acting as a particularly sensitive marker of energy stress [46]. The pronounced accumulation of GDP and AMP under rotenone challenge indicated disrupted nucleotide phosphorylation balance and impaired energy turnover. Our data demonstrated that exogenous succinate rescued aberrant GDP and AMP levels in PD mice, suggesting that succinate alleviated adaptive energetic stress and stabilized mitochondrial nucleotide homeostasis. Notably, although succinate corrected these energy-stress markers, no significant change in ATP and GTP concentrations were observed in the present study. This observation implies that succinate may mitigate energetic stress not by simply boosting steady-state ATP pools, but by restoring the balance of purine nucleotide phosphorylation status. These findings supported the notion that succinate ameliorates certain aspects of energy deficits [48]. However, since dynamic metabolic flux and the catalytic activities of core metabolic enzymes were not directly quantified herein, the precise regulatory cascade underpinning these metabolic changes awaits further experimental validation.

The PI3K/Akt/mTOR pathway is a highly conserved signaling axis that integrates growth factor signals and nutrient availability to govern cellular metabolism, protein synthesis, and survival [49]. This pathway is closely linked to mitochondrial energy metabolism. Insulin-activated Akt can translocate to the mitochondrial membrane, influencing mitochondrial oxidative phosphorylation and bioenergetics in the streptozotocin-induced diabetic mice [50]. Downstream mTOR stimulates mitochondrial biogenesis and activity, and inhibition of mTOR leads to impaired mitochondrial function and glycolysis in PP242-treated MCF7 cells [51]. In PD, dopaminergic neurons display compromised PI3K/Akt/mTOR signaling, which impairs nutrient sensing and mitochondrial bioenergetics, ultimately driving neuronal energy depletion [52]. In rotenone-exposed SH-SY5Y cells, growth/differentiation factor-15 preserves energy metabolism, including maintenance of mitochondrial membrane potential and ATP generation, through activation of the PI3K/Akt/mTOR pathway [53].

A study indicates that succinate may promote macrophage phenotypic polarization by activating the PI3K/Akt signaling pathway, thereby accelerating the progression of necrotizing enterocolitis[54]. Beyond immune regulation, our subsequent validation experiments indicated that exogenous succinate supplementation restored the activity of the PI3K/Akt/mTOR signaling cascade in both the central nervous system and peripheral gut tissues of PD mice. These findings further corroborate the role of the PI3K/Akt/mTOR cascade in regulating energy metabolism in gut and brain. Collectively, activation of the PI3K/Akt/mTOR pathway constitutes a core molecular mechanism by which succinate remodels energy homeostasis, ameliorates intestinal and neuronal metabolic dysfunction, and alleviates PD-related pathological deficits.

5. Conclusion

Taken together, our study demonstrated early GI dysfunction, gut microbial dysbiosis, and TCA cycle disruption as key pathological and metabolic features of PD. Succinate bridged gut dysbiosis and host energy defects. Exogenous succinate supplementation drove metabolic remodeling and alleviated energy metabolic disturbance, motor deficits, and PD pathological phenotypes via activation of the PI3K/Akt/mTOR signaling pathway. These findings delineated a mechanistic framework underlying microbiota–host metabolic crosstalk in PD pathogenesis and suggested succinate as a promising metabolic target. However, further studies are needed to dissect how succinate modulates energy metabolism in PD.

Authorship contribution statement

YJ and SC: Writing -Original Draft. **JS:** Writing -Original Draft, Funding Acquisition. **MZ:** Conceptualization. **SZ:** Conceptualization. **JW:** Conceptualization. **YD:** Conceptualization. **HM:** Conceptualization. **JW:** Conceptualization. **RY:** Conceptualization. **HG:** Conceptualization. **JW:** Conceptualization. **ZW:** Conceptualization. **CC:** Conceptualization. **YY:** Conceptualization. **FL:** Conceptualization. **XB:** Supervision. **CZ:** Supervision, Project administration, Funding acquisition. **DZ:** Supervision, Project administration, Funding acquisition.

Conflict of interest

The authors have no conflict of interest to disclose.

Funding

This work was supported by National Natural Science Foundation of China (No. 82674997), Beijing Science Foundation (No. L246065, 7254400), CAMS Innovation Fund for Medical Sciences (CIFMS) (No. 2026-I2M-SXZX12-04), the National Key Research and Development Program of China (No. 2024YFA0919904), Lingang National Laboratory Project (LGL-2614-11), Open Research fund of State Key Laboratory of Druggability Evaluation and Systematic Translational Medicine (Tianjin Institute of Pharmaceutical Research) (No.712025007), and Beijing Natural Science Foundation (Grant No. 7254400).

Data Availability：

The 16S rRNA amplicon raw sequencing datasets generated and analysed in this study are available in the NCBI Sequence Read Archive (SRA) repository under BioProject accession PRJNA1562285. The RNA-seq transcriptomic raw datasets generated and analyzed in this study are available in the Genome Sequence Archive (GSA) repository under accession subCRA088161. The proteomic raw datasets generated and analyzed in this study have been submitted to the iProX repository under accession IPX002128800.

Reference

1. Morris HR, Spillantini MG, Sue CM, Williams-Gray CH: **The pathogenesis of Parkinson's disease**. *Lancet* 2024, **403**(10423):293-304.
2. Liu M, Jiao Q, Du X, Bi M, Chen X, Jiang H: **Potential Crosstalk Between Parkinson's Disease and Energy Metabolism**. *Aging Dis* 2021, **12**(8):2003-2015.
3. Chen L, Wang C, Qin L, Zhang H: **Parkinson's disease and glucose metabolism impairment**. *Translational Neurodegeneration* 2025, **14**(1):10.
4. Li H, Zeng F, Huang C, Pu Q, Thomas ER, Chen Y, Li X: **The potential role of glucose metabolism, lipid metabolism, and amino acid metabolism in the treatment of Parkinson's disease**. *CNS Neuroscience & Therapeutics* 2024, **30**(2):e14411.
5. Gibson GE, Kingsbury AE, Xu H, Lindsay JG, Daniel S, Foster OJF, Lees AJ, Blass JP: **Deficits in a tricarboxylic acid cycle enzyme in brains from patients with Parkinson's disease**. *Neurochemistry International* 2003, **43**(2):129-135.
6. Yang S, Tian C, Peng D: **Specific gut microbiota alterations and metabolic deficits in Parkinson's disease: a controlled comparison with functional constipation**. *Front Cell Infect Microbiol* 2026, **16**:1767241.
7. den Besten G, van Eunen K, Groen AK, Venema K, Reijngoud DJ, Bakker BM: **The role of short-chain fatty acids in the interplay between diet, gut microbiota, and host energy metabolism**. *J Lipid Res* 2013, **54**(9):2325-2340.
8. Morais LH, Stiles L, Freeman M, Oguienko AD, Hoang JD, Ji J, Jones J, Quan B, Devine J, Bois JS *et al*: **The gut microbiome promotes mitochondrial respiration in the brain of a Parkinson's disease mouse model**. *NPJ Parkinsons Dis* 2025, **11**(1):301.
9. Bajpai P, Darra A, Agrawal A: **Microbe-mitochondrion crosstalk and health: An emerging paradigm**. *Mitochondrion* 2018, **39**:20-25.
10. Mao L, Zhang Y, Tian J, Sang M, Zhang G, Zhou Y, Wang P: **Cross-Sectional Study on the Gut Microbiome of Parkinson's Disease Patients in Central China**. *Front Microbiol* 2021, **12**:728479.
11. Guo X, Tang P, Hou C, Chong L, Zhang X, Liu P, Chen L, Liu Y, Zhang L, Li R: **Integrated Microbiome and Host Transcriptome Profiles Link Parkinson's Disease to Blautia Genus: Evidence From Feces, Blood, and Brain**. *Front Microbiol* 2022, **13**:875101.
12. Wei YH, Ma X, Zhao JC, Wang XQ, Gao CQ: **Succinate metabolism and its regulation of host-microbe interactions**. *Gut Microbes* 2023, **15**(1):2190300.
13. Wang YD, Bao XQ, Xu S, Yu WW, Cao SN, Hu JP, Li Y, Wang XL, Zhang D, Yu SS: **A Novel Parkinson's Disease Drug Candidate with Potent Anti-neuroinflammatory Effects through the Src Signaling Pathway**. *J Med Chem* 2016, **59**(19):9062-9079.
14. Oroszi T, Geerts E, de Boer SF, Schoemaker RG, van der Zee EA, Nyakas C: **Whole Body Vibration Improves Spatial Memory, Anxiety-Like Behavior, and Motor Performance in Aged Male and Female Rats**. *Front Aging Neurosci* 2021, **13**:801828.
15. McQuade RM, Singleton LM, Wu H, Lee S, Constable R, Di Natale M, Ringuet MT, Berger JP, Kauhausen J, Parish CL *et al*: **The association of enteric neuropathy with gut phenotypes in acute and progressive models of Parkinson's disease**. *Sci Rep* 2021, **11**(1):7934.
16. Liu L, Zhao Y, Yang W, Han L, Mo X, Sheng J, Tian Y, Gao X: **Correlations Between Amelioration of Rotenone-Induced Parkinson's Symptoms by Amomum tsaoko**

Flavonoids and Gut Microbiota in Mice. *Int J Mol Sci* 2025, **26**(4).

17. Elford JD, Becht N, Garssen J, Kraneveld AD, Perez-Pardo P: **Buty and the beast: the complex role of butyrate in Parkinson's disease**. *Front Pharmacol* 2024, **15**:1388401.
18. Litvak Y, Byndloss MX, Bäumler AJ: **Colonocyte metabolism shapes the gut microbiota**. *Science* 2018, **362**(6418).
19. Wang K, Liao M, Zhou N, Bao L, Ma K, Zheng Z, Wang Y, Liu C, Wang W, Wang J: **Parabacteroides distasonis alleviates obesity and metabolic dysfunctions via production of succinate and secondary bile acids**. *Cell reports* 2019, **26**(1):222-235. e225.
20. Döring C, Basen M: **Propionate production by Bacteroidia gut bacteria and its dependence on substrate concentrations differs among species**. *Biotechnology for biofuels and bioproducts* 2024, **17**(1):95.
21. Gindt ME, Lück R, Deppenmeier U: **Genetic optimization of the human gut bacterium Phocaeicola vulgatus for enhanced succinate production**. *Appl Microbiol Biotechnol* 2024, **108**(1):465.
22. Tingler AM, Engevik MA: **Breaking down barriers: is intestinal mucus degradation by Akkermansia muciniphila beneficial or harmful?** *Infection and Immunity* 2025, **93**(9):e00503-00524.
23. Kirmiz N, Galindo K, Cross KL, Luna E, Rhoades N, Podar M, Flores GE: **Comparative Genomics Guides Elucidation of Vitamin B(12) Biosynthesis in Novel Human-Associated Akkermansia Strains**. *Appl Environ Microbiol* 2020, **86**(3).
24. Pellegrino A, Coppola G, Santopaolo F, Gasbarrini A, Ponziani FR: **Role of Akkermansia in Human Diseases: From Causation to Therapeutic Properties**. *Nutrients* 2023, **15**(8).
25. Janssen PH, Schuhmann A, Mörschel E, Rainey FA: **Novel anaerobic ultramicrobacteria belonging to the Verrucomicrobiales lineage of bacterial descent isolated by dilution culture from anoxic rice paddy soil**. *Appl Environ Microbiol* 1997, **63**(4):1382-1388.
26. Zaunmuller T, Kelly DJ, Glockner FO, Unden G: **Succinate dehydrogenase functioning by a reverse redox loop mechanism and fumarate reductase in sulphate-reducing bacteria**. *Microbiology* 2006, **152**(8):2443-2453.
27. Lewis AJ, Miller JD: **Keto acid metabolism in Desulfovibrio**. *J Gen Microbiol* 1975, **90**(2):286-292.
28. Xu K, Zhu S, Ma J, Zu M, Yang J, Xu F, Dai L, Liu D, Wang Y, Zhang X *et al*: **PI3K/Akt/mTOR signaling pathway mediates energy metabolic reprogramming and regulates mitochondrial homeostasis in host cells exposed to Toxoplasma gondii**. *Microbiology Spectrum* 2025, **14**(2):e01385-01325.
29. Braak H, de Vos RA, Bohl J, Del Tredici K: **Gastric alpha-synuclein immunoreactive inclusions in Meissner's and Auerbach's plexuses in cases staged for Parkinson's disease-related brain pathology**. *Neurosci Lett* 2006, **396**(1):67-72.
30. Fang X, Liu S, Muhammad B, Zheng M, Ge X, Xu Y, Kan S, Zhang Y, Yu Y, Zheng K *et al*: **Gut microbiota dysbiosis contributes to α-synuclein-related pathology associated with C/EBPβ/AEP signaling activation in a mouse model of Parkinson's disease**. *Neural Regeneration Research* 2024, **19**(9).
31. Huang B, Chau SWH, Liu Y, Chan JWY, Wang J, Ma SL, Zhang J, Chan PKS, Yeoh YK, Chen Z *et al*: **Gut microbiome dysbiosis across early Parkinson's disease, REM sleep**

behavior disorder and their first-degree relatives. *Nature Communications* 2023, **14**(1):2501.

32. Jiao X, Li H, Wang T, Fu H, Wang S, Liu H, Wang L, Li X, Deng A, Li Z: **Progressive gut microbiota shifts and functional alterations across aging stages and frailty in mice**. *iScience* 2025, **28**(7):112985.
33. Nishida A, Ando Y, Kimura I, Miyamoto J: **Involvement of Gut Microbial Metabolites Derived from Diet on Host Energy Homeostasis**. In: *International Journal of Molecular Sciences*. vol. 23; 2022: 5562.
34. Kim S, Seo S-U, Kweon M-N: **Gut microbiota-derived metabolites tune host homeostasis fate**. In: *Seminars in immunopathology: 2024*: Springer; 2024: 2.
35. Wang J, Zhu N, Su X, Gao Y, Yang R: **Gut-Microbiota-Derived Metabolites Maintain Gut and Systemic Immune Homeostasis**. In: *Cells*. vol. 12; 2023: 793.
36. Li T-T, Chen X, Huo D, Arifuzzaman M, Qiao S, Jin W-B, Shi H, Li XV, Iliev ID, Artis D *et al*: **Microbiota metabolism of intestinal amino acids impacts host nutrient homeostasis and physiology**. *Cell Host & Microbe* 2024, **32**(5):661-675.e610.
37. Corbin KD, Carnero EA, Dirks B, Igudesman D, Yi F, Marcus A, Davis TL, Pratley RE, Rittmann BE, Krajmalnik-Brown R *et al*: **Host-diet-gut microbiome interactions influence human energy balance: a randomized clinical trial**. *Nature Communications* 2023, **14**(1):3161.
38. Cheng J, Hu J, Geng F, Nie S: **Bacteroides utilization for dietary polysaccharides and their beneficial effects on gut health**. *Food Science and Human Wellness* 2022, **11**(5):1101-1110.
39. Cohen LB, Lindsay SA, Xu Y, Lin SJH, Wasserman SA: **The Daisho Peptides Mediate Drosophila Defense Against a Subset of Filamentous Fungi**. *Front Immunol* 2020, **11**:9.
40. Cerroni R, Pietrucci D, Teofani A, Chillemi G, Liguori C, Pierantozzi M, Unida V, Selmani S, Mercuri NB, Stefani A: **Not just a Snapshot: An Italian Longitudinal Evaluation of Stability of Gut Microbiota Findings in Parkinson's Disease**. *Brain Sci* 2022, **12**(6).
41. Singh Y, Trautwein C, Romani J, Salker MS, Neckel PH, Fraccaroli I, Abeditashi M, Woerner N, Admard J, Dhariwal A *et al*: **Overexpression of human alpha-Synuclein leads to dysregulated microbiome/metabolites with ageing in a rat model of Parkinson disease**. *Mol Neurodegener* 2023, **18**(1):44.
42. Murphy MP, Chouchani ET: **Why succinate? Physiological regulation by a mitochondrial coenzyme Q sentinel**. *Nat Chem Biol* 2022, **18**(5):461-469.
43. Akbar M, Yadav S, Naseer A, Hameed R, Sarkar A, Nazir A: **Gut microbiota-derived succinate links proteostasis collapse to α-synuclein pathology and aging**. *iScience* 2026, **29**(6):115941.
44. Zeevalk GD, Manzino L, Hoppe J, Sonsalla P: **In vivo vulnerability of dopamine neurons to inhibition of energy metabolism**. *Eur J Pharmacol* 1997, **320**(2-3):111-119.
45. Semenovich D, Lukiyenko E, Titko O, Kanunnikova N: **Panthenol and succinate as modulators of changes of redox balance and energy metabolism in the experimental model of Parkinson's disease**. *Ind J Appl Res* 2018, **8**:436-438.
46. Hardie DG: **AMP-activated protein kinase: a cellular energy sensor with a key role in metabolic disorders and in cancer**. *Biochem Soc Trans* 2011, **39**(1):1-13.
47. Fujisawa K, Wakazaki M, Matsuzaki A, Matsumoto T, Yamamoto N, Noma T, Takami T:

Adenylate Kinase Isozyme 3 Regulates Mitochondrial Energy Metabolism and Knockout Alters HeLa Cell Metabolism. *Int J Mol Sci* 2022, **23**(8).

48. Nowak G, Clifton GL, Bakajsova D: **Succinate ameliorates energy deficits and prevents dysfunction of complex I in injured renal proximal tubular cells**. *J Pharmacol Exp Ther* 2008, **324**(3):1155-1162.
49. Saxton RA, Sabatini DM: **mTOR Signaling in Growth, Metabolism, and Disease**. *Cell* 2017, **168**(6):960-976.
50. Yang JY, Yeh HY, Lin K, Wang PH: **Insulin stimulates Akt translocation to mitochondria: implications on dysregulation of mitochondrial oxidative phosphorylation in diabetic myocardium**. *J Mol Cell Cardiol* 2009, **46**(6):919-926.
51. Morita M, Gravel SP, Chénard V, Sikström K, Zheng L, Alain T, Gandin V, Avizonis D, Arguello M, Zakaria C *et al*: **mTORC1 controls mitochondrial activity and biogenesis through 4E-BP-dependent translational regulation**. *Cell Metab* 2013, **18**(5):698-711.
52. Reich N, Hölscher C: **The neuroprotective effects of glucagon-like peptide 1 in Alzheimer's and Parkinson's disease: An in-depth review**. *Front Neurosci* 2022, **16**:970925.
53. Li P, Lv H, Zhang B, Duan R, Zhang X, Lin P, Song C, Liu Y: **Growth Differentiation Factor 15 Protects SH-SY5Y Cells From Rotenone-Induced Toxicity by Suppressing Mitochondrial Apoptosis**. *Front Aging Neurosci* 2022, **14**:869558.

Supplementary Files

This is a list of supplementary files associated with this preprint. Click to download.

- Supplementaryinformation.docx
- SupplymentaryfileGelsandBlots.zip